

Wearable Textile-based Dual-band 8-element Rectenna Array for Polarization Independent Far-field RF Energy Harvesting

Nasir Ullah Khan, *Graduate Student Member, IEEE*, Abdul Basir, *Member, IEEE*, Arcangelo Merla, and Toni Björninen, *Senior Member, IEEE*

Abstract—This study introduces a dual-band wearable 8-element rectenna for self-powered wearable sensors based on far-field RF energy harvesting at 2.45 and 5.8 GHz. The array was patterned on a textile substrate by laser-cutting a conductive textile and tested in body-worn configuration for both radiation pattern and RF-to-DC conversion properties. It comprises eight monopole-type dual-band element antennas, arranged in a circular configuration that ensures 50% combined mutual polarization efficiency with an incident electromagnetic wave impinging on it regardless of the wave's polarization. Single element exhibits the gain of 2.5 dBi at 2.45 GHz and 5.7 dBi at 5.8 GHz with the corresponding input reflection coefficients below -15 dB in the body-worn configuration. The mutual coupling between the elements remains well below -20 dB at both operating frequencies. With the serial-type DC-combining approach, this yielded a stable 1.8 V output DC voltage from the rectenna array over a 4 k Ω load.

Keywords—Energy harvesting, polarization diversity, rectenna, rectifier, wearable electronics.

I. INTRODUCTION

DIGITAL healthcare solutions and real-time monitoring systems are crucial for the elderly, disabled, and individuals with mobility challenges, as they help avoid emergencies and improve overall outcomes of care [1]. Recently, wearable devices that monitor physiological data have attracted significant attention owing to their adaptability, scalability, and user-friendly design [2]. Among these, skin-inspired wearable devices that conform to the body provide greater stability and precision in capturing critical data, such as temperature, pressure, pH levels, strain, and acceleration [3], [4], [5]. The demand for continuous and efficient monitoring necessitates the wearable devices to be powered by a long-lasting, reliable, and uninterrupted energy source [6]. However, conventional wearable devices rely predominantly on rigid electro-chemical batteries to provide consistent power. This approach poses several challenges, including limited operational lifespan and high maintenance costs [7]. Moreover, the inflexible structure of regular batteries limits the possibility of creating devices that conform to the body, reducing the user's comfort. Beyond these limitations, batteries pose safety hazards, including the risk of chemical leakage, overheating, or even explosions [8]. In addition, improper disposal of these chemical batteries can contribute to environmental pollution, causing issues related to electronic waste [9]. These challenges underscore the demand for innovative energy solutions that are reliable, safe, and environmentally sustainable, aligning with the developing demand for next generation wearable devices [10].

This work was supported by funding from the Italian National Recovery and Resilience Plan (PNRR) project and partially supported by Abdul Basir and Toni Björninen, funded by the Research Council of Finland (funding decision: 349422).

Nasir Ullah Khan and Arcangelo Merla is with the Department of Engineering and Geology, University "G. d'Annunzio" Chieti-Pescara, 65127 Pescara, Italy

Abdul Basir and Toni Björninen are with Tampere Electronics Research Centre, Tampere University, Tampere, 33720 Finland.

Reliable and uninterrupted power sources can be realized through green energy technologies, which provide a self-powered, battery-free system capable of consistent monitoring and diagnostics. The primary green energy sources include piezoelectric, photovoltaic, hydropower, thermal, electrostatic, and both near-field and far-field RF energy [11], [12], [13], [14], [15], [16], [17]. However, integrating these into wearable devices poses challenges. Photovoltaics rely on light, resulting in low power output during low-light conditions. Electrostatic and piezoelectric systems require mechanical deformation or robust physical activity, which may be impractical for elderly or immobile individuals. Near-field electromagnetic radiation depends on the precise alignment between the transmitter and receiver and may pose safety concerns. In remote health monitoring, fluctuating environmental factors such as light, temperature, time of day, and weather can disrupt power generation, potentially compromising device functionality [18] [19]. Therefore, a reliable and user-friendly power source is essential for wearables, allowing effective virtual healthcare monitoring [20].

Far-field RF energy harvesting (RFEH) utilizes electromagnetic energy from various sources, including licensed communication bands and unlicensed ISM bands. Commercial products such as biomedical equipment, routers, and WiFi systems contribute to ambient RF energy, highlighting its versatility and reliability to power wearables [21]. Currently, RF transmitters deployed in various smart environments, such as offices, homes, hospitals, and transportation systems, radiate appreciable amounts of RF energy. In addition, advancements in 5G communications further enhance the feasibility of RF harvesting. Implementing an RFEH system provides numerous advantages: it can be compact, cost-effective, and reliable, with RF residues widely accessible regardless of changing environmental factors such as temperature, humidity, or weather [22].

RFEH system requires a rectenna, which comprises an antenna and a rectifier circuit to effectively convert ambient RF

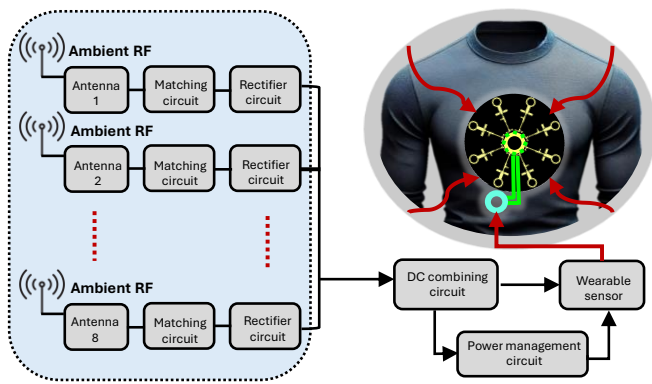


Fig. 1. Block diagram of the proposed 8-element rectenna for powering wearable sensors.

residues into useful DC. Recently, significant efforts have been made to utilize RF energy harvesting techniques to power low-power devices. Nevertheless, effective utilization of the RFEH system poses challenges such as low RF-to-DC power conversion efficiency (PCE), primarily caused by a low ambient RF power density, resulting in low energy output. To address these challenges, multiband antennas and antenna arrays are proposed for RFEH, which presents notable outcomes [23] [24]. Single-port array antennas need an additional feeding circuit to excite each element, which can insert additional losses due to the complex circuit [25]. These losses have a notable impact in the field of RFEH, where efficiency is crucial. Moreover, high gain and wide beamwidth are always a trade-off in such arrays [26]. As a result, multipoint arrays are generally more suited options for harvesting ambient RF energy. However, combining the energy harvested from such arrays presents its own set of challenges. Both the DC and RF combining methods have been analyzed [27], with results indicating that DC combining provides distinct features. In particular, DC combining can provide a wide beamwidth, allowing the reception of ambient RF signals from a wider range, while maintaining a high gain simultaneously [28].

In [29], a multi-sector planar rectenna array with uniform 3D spherical coverage for the IoT sensor nodes was proposed. However, the integration of a central boresight and multiple end-fire antennas increases fabrication complexity, and its sensitivity to diode impedance variations with input power and single-band operation limits its adaptability. In [30], a circular multibeam array composed of Vivaldi antennas integrated with rectifiers was proposed. It provides multiple beams and consistently high gain across the harvesting bands with omnidirectional pattern. Although the harvester ensures continuous power to IoT devices, its relatively large footprint ($460 \times 460 \text{ mm}^2$) poses a challenge to integration with compact wearable sensors. Notably, the previously mentioned harvesters were manufactured on a rigid substrate, which complicates their implementation on wearable materials for integration with wearable sensors.

A textile-based harvester embroidered on a cotton substrate featuring a five-element array [31], demonstrated stable harvesting performance but was embroidered on a relatively large

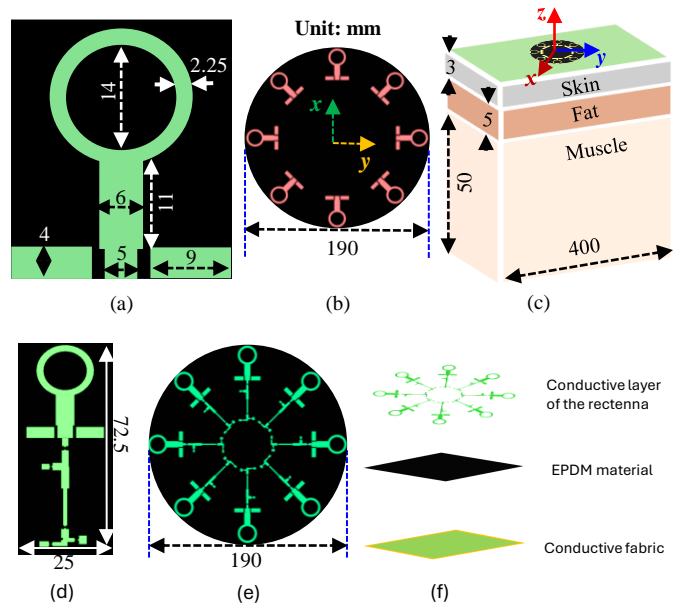


Fig. 2. Proposed 8-element rectenna (a) single monopole element, (b) 8-elements array configuration, (c) simulation setup, (d) rectifier integrated single element, (e) rectifier integrated 8-element array, (f) layers involved in the design. unit: mm

area ($240 \times 240 \text{ mm}^2$) and was limited to operate at 2.45 GHz band only.

To address the existing challenges of compactness, harvested power efficiency, integration with wearables, and flexibility in RFEH applications, we propose a textile-based rectenna array featuring polarization robustness. The harvester features eight monopole elements with dual-band characteristics, arranged in a circular configuration, eliminating the need for a complex feeding network with compactness and flexibility suitable for wearable devices.

This work extends our preliminary study in [32], which focused solely on the design of dual-band antenna arrays. However, the current manuscript significantly extends it by including on-body radiation characterization, rectifier design and optimization, and complete system-level validation of the proposed system. Moreover, the proposed system introduces polarization robustness and angular coverage while maintaining stable DC voltage levels.

The block diagram of the proposed multipoint rectenna is presented in Fig. 1. This configuration of the elements offers distinct advantages: inherent polarization diversity, which ensures wide angular coverage and stable performance of the rectenna regardless of the transmitter's location. This orientation confirms that, at any given time, only two elements might experience cross-polarization with a linearly transmitted wave, while the remaining six elements maintain efficient reception. This distinct feature enhances the reliability of the design in ambient RF environments where source positions and signal polarization might be varied. Moreover, the serial DC combining circuit raises the total output voltage and provides a consistent power supply.

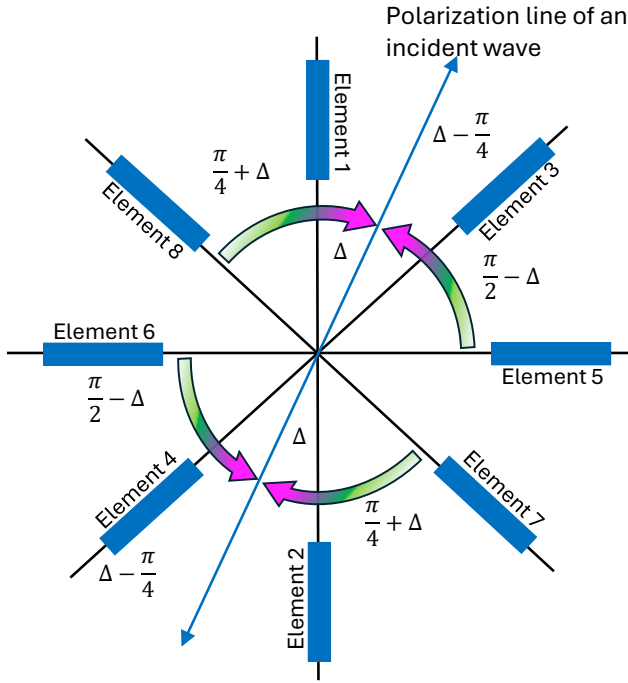


Fig. 3. Schematic of general structural consideration of the proposed 8-element rectenna.

II. METHODS

This section describes the antenna and circuit design principles, simulation environments, and materials and manufacturing methods used to implement the dual-band rectenna array prototype for experiments.

A. General Structural Considerations

The proposed rectenna array comprises eight identical circular ring monopoles fed with coplanar waveguides. The elements are placed at 45° angular separation around a fixed center point, as shown in Fig. 2(a-b). The rectenna development was initiated by optimizing the wearable textile-based antennas (Fig. 2(a)) to operate at two ISM bands centered at 2.45 and 5.8 GHz. After optimizing the dual-band monopole element antenna, the total number of antennas for the rectenna was selected considering that a large number of antennas provides a higher likelihood for good polarization matching with an incident linearly polarized EM wave, but too dense spacing would lead to increased mutual coupling between the antennas such that their impedance matching could no longer be optimized independently. Through simulations, it was found that eight elements provided a suitable balance between polarization coverage and mutual coupling.

Since a monopole antenna is linearly polarized, with the electric field vector aligned along the monopole's axis, in the proposed circular configuration with eight antennas, there is always a pair of monopoles at 180° separation that have good mutual polarization efficiency with a linearly polarized incident electromagnetic wave. Consequently, an orthogonal pair of monopoles would be nearly cross-polarized, and the

four remaining monopoles would exhibit a mutual polarization efficiency close to 50% with the incident wave.

The total polarization efficiency of the rectenna, considering all the antennas as linearly polarized impinges on it, can be analyzed using the diagram shown in Fig. 3. From the diagram, the polarization efficiency (PE) for a linearly polarized antenna is given by [33]

$$PE = \cos^2(\Delta), \quad (1)$$

where we can assume $0 < \Delta \leq \pi/4$. This is true since if $\Delta > \pi/4$, due to the rotational symmetry of the rectenna, we could always renumber the monopoles so that $0 < \Delta \leq \pi/4$ for a new monopole number 1. Therefore,

$$PE_1 = PE_2 = \cos^2(\Delta) \quad (2)$$

for the monopoles 1 and 2 in the diagram. Further, for monopoles 3 and 4 we can write

$$\begin{aligned} PE_3 = PE_4 &= \cos^2\left(\Delta - \frac{\pi}{4}\right) \\ &= \frac{1}{2}(\cos \Delta + \sin \Delta)^2 \end{aligned} \quad (3)$$

where the last equality follows from the sum of angles formula for cosine. Similarly,

$$PE_5 = PE_6 = \cos^2\left(\frac{\pi}{2} - \Delta\right) = \sin^2(\Delta) \quad (4)$$

for the monopoles 5 and 6. Lastly,

$$\begin{aligned} PE_7 = PE_8 &= \cos^2\left(\frac{\pi}{4} + \Delta\right) \\ &= \frac{1}{2}(\cos \Delta - \sin \Delta)^2 \end{aligned} \quad (5)$$

for the monopoles 7 and 8, where the sum of angles formula for cosine was used to obtain the last equality. Now, we can sum up the efficiencies of the monopoles to obtain

$$\begin{aligned} PE_{\text{tot}} &= \sum_{k=1}^8 PE_k = \underbrace{2\cos^2(\Delta) + 2\sin^2(\Delta)}_{=2} \\ &+ \underbrace{(\cos \Delta + \sin \Delta)^2 + (\cos \Delta - \sin \Delta)^2}_{=2} = 4, \end{aligned} \quad (6)$$

which holds regardless of the value of Δ . Thus, the 8-element rectenna maintains the 50% total mutual polarization efficiency regardless of the polarization tilt angle Δ of an incident linearly polarized wave relative to the rectenna. Since any elliptically polarized EM wave can be given as a superposition of two linearly polarized waves, the same total efficiency holds for a general elliptically polarized incident wave.

B. Wearable Dual-band Monopole Antenna

The antenna development was completed utilizing Ansys HFSS based on the finite element method. To establish the baseline performance, initial simulations were conducted in free space, followed by further optimization of a single antenna on a simplified human body phantom. As shown in Fig. 2(c), the 3-layer homogeneous body phantom used in the simulations consists of skin, fat, and muscle with the dimensions of $400 \times 400 \times 58 \text{ mm}^3$ representing the average size of the upper

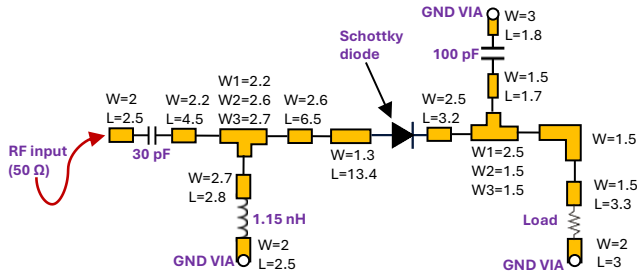


Fig. 4. Schematic of the designed dual-band rectifier circuit with detailed parameters. unit: mm

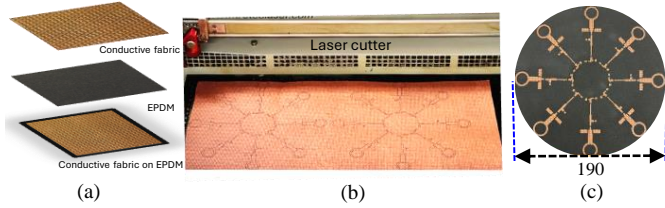


Fig. 5. Overview of the fabrication procedure: (a) prefabrication setup of the materials, (b) laser cutting of the prototype, (c) rectenna array prototype.

body of an adult person. The frequency-dependent relative permittivity and conductivity of human tissues are assigned to the phantom based on the data provided in [34]. After achieving an appropriate performance for a single wearable antenna, we studied the mutual coupling between several of them arranged to a rotation-symmetric grid and concluded that to maintain low mutual coupling between the adjacent antennas, we need to limit the number of antennas to eight. Finally, we included 50Ω SMA connectors to the feed line of each antenna to account for the electromagnetic connector-to-antenna transition effects that are present in the manufactured prototype in antenna measurements.

C. Dual-band Rectifier

A rectifier is a pivotal component of an RFEH system, responsible for converting ambient RF energy into usable DC power to energize electronic devices. Designing an efficient and reliable dual-band diode-based rectifier is inherently complex and poses significant challenges due to the non-linear behavior of the diode, making the circuit's input impedance power-dependent. For optimal efficiency, a single-diode rectifier was chosen, as in RFEH, multiple-diode-based rectifiers often lead to reduce efficiency due to higher diode losses [30]. We selected the rectifier's diode to be SMS7621 from Skyworks [35], based on its excellent characteristics for the application: low forward voltage drop, minimal junction capacitance, low series resistance, and high sensitivity at low power levels critical for RFEH applications [36]. The rectifier was fully designed using Keysight ADS software. The circuit diagram of the proposed dual-band rectifier, operating at ISM bands 2.45 and 5.8 GHz, is shown in Fig. 4. An impedance matching circuit composed of a serial microstrip

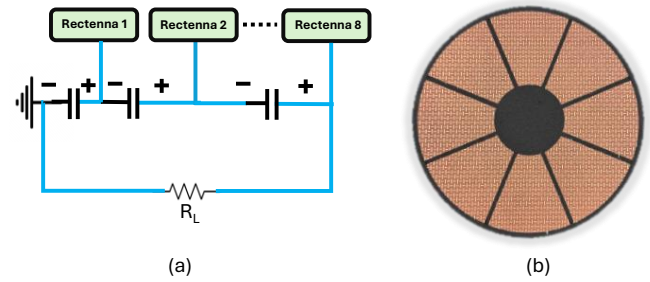


Fig. 6. Proposed DC combining circuit (a) block diagram of serial DC combining, (b) isolated ground plane of the rectifiers.

line, a shunt inductor, and a shunt short-circuited stub converts the rectifier's low-resistance and capacitive impedance to 50Ω at both operating frequencies at low input power levels ($-20 \dots 0$ dBm) relevant to the RFEH system.

D. Manufacturing

The manufacturing of the rectenna array was carried out using a Trotec CO2 Laser System 60W. This tool provides fine resolution and high precision, which are essential for wearable applications. The antenna substrate is Ethylene Propylene Diene Monomer (EPDM), which is a synthetic textile with a dielectric constant of 1.534 and a loss tangent of 0.01 [37]. EPDM was selected due to its flexibility, inexpensiveness, toughness, durability, and ability to withstand the high temperature [38] required during the soldering of components to the rectenna prototype. Shieldex Kiel-SK-96, a copper-nylon conductive fabric with a thickness of 0.56 mm and a surface resistivity of $0.02 \Omega/\text{Sq}$. [39], forms the radiating element of the antenna as shown in Fig. 5. The CAD file of the array was uploaded to the laser cutter interface and the laser head was focused on the appropriate distance from the material ensuring optimal precision. For this project, the cut settings; power, speed and frequency of the laser beam were selected to 100, 10, 1000 respectively, ensuring even and precise cutting process. Following the cutting, the conductive fabric having a hot melt adhesive layer on one side was carefully ironed onto the substrate.

E. DC Combining Circuit

The DC output from the rectifiers is summed up over a common load via a serial DC combining circuit shown in Fig. 6a. While the approach does not improve the RF-to-DC efficiency of the individual rectifiers, it helps generate a higher DC voltage from the same incident power density as compared with RF combining and a single rectifier. Although advanced techniques such as multi-input-multi-output (MIMO) switching DC-DC converters, as mentioned in [40] and [41], can be utilized to improve the DC combining efficiency further, they add complexity to the circuit. To ensure a simple yet effective method, our system incorporates the serial DC combining method. While the parallel DC combining circuit, used for example in [28], would boost the output DC current, we considered it more relevant to ensure the output DC

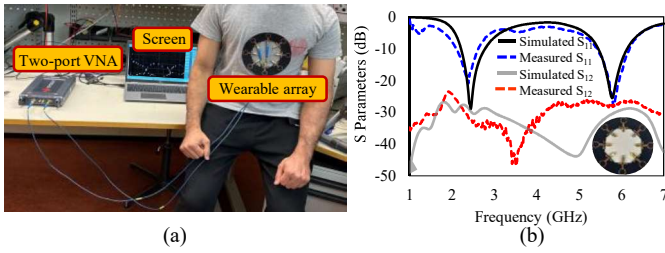


Fig. 7. (a) Experimental setup for the measurement of S-parameters, (b) comparison of simulated and measured S-parameters, indicating close agreement between results. S_{11} shows the reflection coefficient of Ant-1, S_{12} shows the mutual coupling between Ant-1 and Ant-2.

voltage is at a sufficient level for operating voltage-activated semiconductor devices and charging a supercapacitor, for example. A key factor for the serial DC voltage combining is the isolation of the ground planes as shown in Fig. 6b.

III. RESULTS AND DISCUSSION

This section presents the performance assessment of the rectenna based on simulated and measured data. The simulated results include the reflection coefficient and radiation pattern of the developed array, which were confirmed through measurements. Likewise, the performance of the dual-band rectifier was evaluated through simulations in terms of the reflection coefficient, the DC output voltage, and the power conversion efficiency. The simulations were verified through experimental tests to ensure the effectiveness of the proposed harvester. These assessments collectively highlight the rectenna's potential for efficient and reliable ambient RFEH.

A. Scattering Parameters

S-parameters of the developed array were measured in the lab using a two port Keysight P5004B vector network analyzer (VNA). The rectenna was placed on a human volunteer's chest, for a realistic validation, and connected to the VNA through 50Ω connectors to measure the reflection coefficient S_{11} and the mutual coupling between adjacent elements ($S_{12} \dots S_{18}$). The experimental setup for measuring S-parameters is shown in Fig. 7a, while Fig. 7b presents the comparison between the simulated and measured results. The measured results indicate good S_{11} surpassing -15 dB in the two operating frequencies and closely matched frequency trends in the studied 1–7 GHz bandwidth. Moreover, the measured S_{12} is well below -20 dB, ensuring minimal interference between adjacent elements.

Although slight differences can be observed in the simulated and measured frequency trends of S_{12} , the differences occur at very small values between -30 dB and -40 dB, such that they have little practical meaning and can be attributed to measurement uncertainty. The mutual coupling between the non-adjacent elements such as $S_{13}, S_{14}, \dots, S_{18}$ were found to be very small, below -40 dB. Both the simulated and measured S parameter results for S_{11} and S_{12} validate the configuration of the rectenna. The good impedance matching, along with low coupling between adjacent elements, ensures efficient power transfer, making it suitable for RFEH applications.

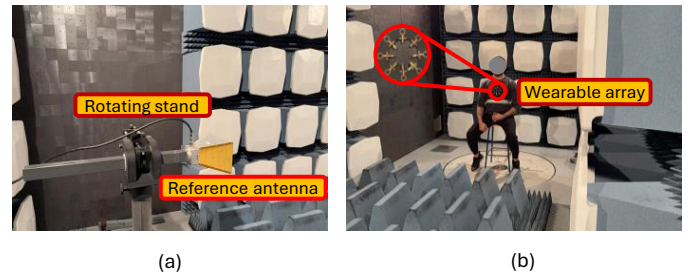


Fig. 8. Experimental setup for measuring radiation patterns, (a) reference antenna, (b) proposed receiver array wore by human volunteer.

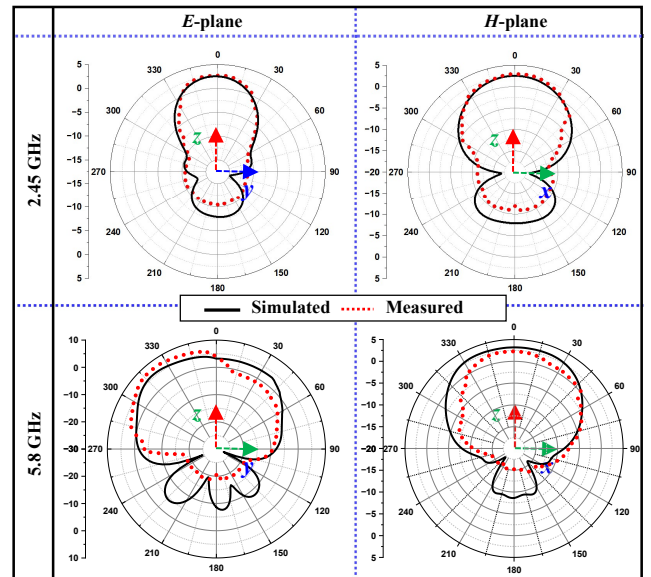


Fig. 9. Comparison of the simulated and measured radiation patterns on human's chest volunteer. E-plane and H-plane figures indicate the examined peak gain values towards the main lobe.

B. Radiation Pattern

To develop an RFEH system, the radiation patterns of the antenna array are significant to analyze. The efficiency of the overall harvesting system is impacted by the way the antenna radiates or receives power in various directions, as determined by the radiation pattern. The antenna measurements were conducted in an anechoic chamber using the reference gain method. According to the design of the proposed rectenna, the elements have a circular symmetric configuration, the radiation pattern of one element was measured while the other elements were terminated with 50Ω terminators. Fig. 8(a) explains the experimental setup employed in the radiation pattern measurement of the wearable antenna array. The array was mounted on the chest of a human volunteer to mimic realistic operational conditions, as shown in Fig. 8(b). A high-gain horn antenna is used as a reference antenna to receive the transmitted signal. To create a complete radiation pattern, measurements were taken at various angles using the reference antenna mounted on a rotation stage.

In the pattern measurement, the reference antenna's was

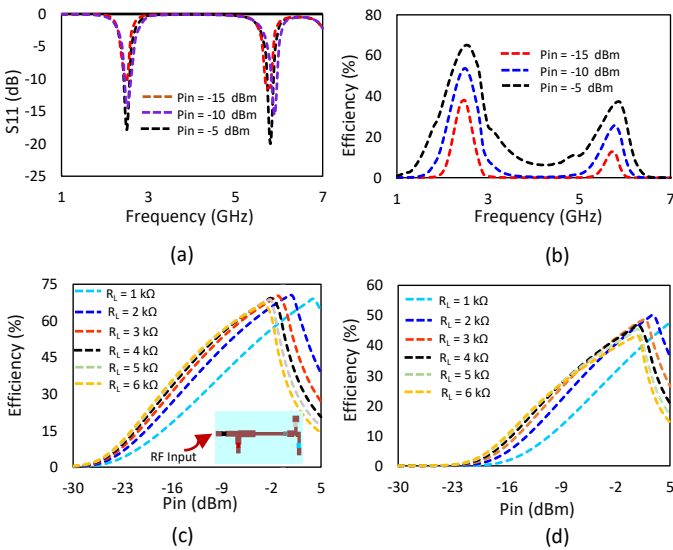


Fig. 10. Simulated performance indicators of the dual-band rectifier, (a) input reflection coefficient, (b) RF-to-DC power conversion efficiency as a function of frequency, (c) RF-to-DC power conversion efficiency for different load resistances at 2.45 GHz, as a function of input power, (d) RF-to-DC power conversion efficiency for different load resistances at 5.8 GHz, as a function of input power.

kept vertical to the wearable monopole antenna to obtain vertical radiation for E-plane polarization measurement. Next, the reference antenna was rotated by 90° to capture the H-plane radiation pattern. The simulated and measured gain at the operating frequencies in the two planes are presented in Fig. 9. The results show that the simulated and measured gain values at the z-axis direction agree closely with the values of 2.5 dBi and 5.7 dBi at 2.45 GHz and 5.8 GHz, respectively. The minor difference between the simulated and measured E-plane pattern at 5.8 GHz could be a result of residual reflections in the chamber or slight asymmetry in the placement of the array with respect to the person wearing it. The differences observed in the backlobe region are most likely explained by the difference between the simplified phantom used in the simulation and the actual measurement scenario.

C. Dual-band Rectifier Analysis

Simulated S_{11} results of the designed rectifier circuit evaluated for low input power levels, ranging from -15 to -5 dBm, are shown in Fig. 10(a), confirming -10 dB bandwidth, indicating efficient impedance matching and minimal reflection losses at both the frequency bands for all the specified input power levels. The rectifier's PCE was analysed as a function of frequency to determine its ability to convert RF into DC power. At 2.45 GHz, the rectifier achieved maximum PCE with 64.9% at -5 dBm, 53.6% at -10 dBm and 37.7% at -15 dBm, as shown in Fig. 10(b). Similarly, at 5.8 GHz, the rectifier gains PCE values of 36.8% at -5 dBm, 25.6% at -10 dBm and 11.5% at -15 dBm. The optimal load resistance was determined to be 4 k Ω , to achieve these values. These results indicate the rectifier's ability to operate reliably across a range of low input power, which is crucial requirement for

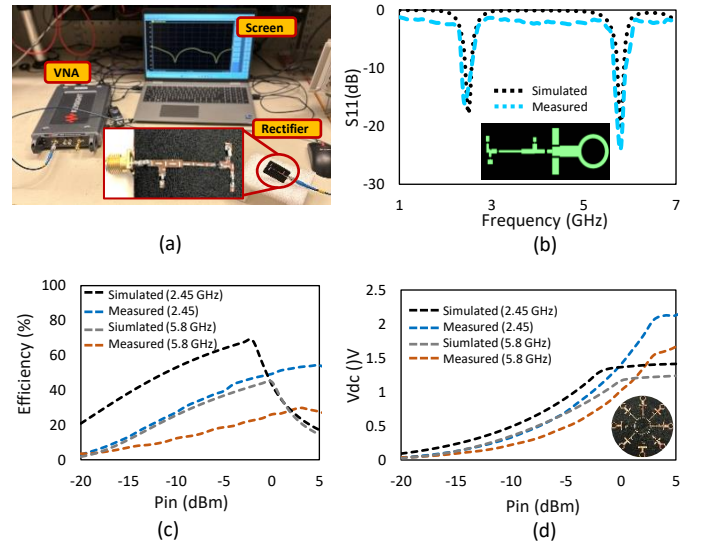


Fig. 11. Experimental analysis of the designed dual-band rectifier, (a) Experimental setup, (b) comparison of the simulated and measured S_{11} , (c) comparison of the simulated and measured RF-to-DC power conversion efficiency as a function of input power, (d) comparison of the simulated and measured output DC voltage levels as a function of input power.

harvesting RF energy. Moreover, variation with input power is shown in Fig. 11(c). At 2.45 GHz, peak efficiency of 68.5% is obtained at -2 dBm while the rectifier's peak efficiency of 44.8% occurs at 0 dBm for 5.8 GHz. These results suggest the rectifier's ability with varying input power, showcasing its reliability for real world energy harvesting applications.

In addition to PCE, the proposed rectifier is evaluated for output DC voltages over a range of input powers as shown in Figure 11(d). At 2.45 GHz, the rectifier achieves output voltage of 0.91 V at -5 dBm and 1.36 V at 0 dBm, while at 5.8 GHz, the respective output voltages are 0.68 V and 1.16 V at -5 dBm and 0 dBm respectively. These findings highlight that even at low input power levels, the rectifier can produce viable voltage levels for powering low-power wearable sensors.

To further examine the rectifier's performance, PCE is analysed at 2.45 GHz (Fig. 10(c)) and 5.8 GHz (Fig. 10(d)), for a range of load resistance, spanning from 1 to 6 k Ω . This analysis assures the rectifier's adaptability to various application scenarios, where the load resistance may vary according to the device being powered. Figure 11(a) presents the experimental setup employed for rectifier characterization. The simulated and measured S_{11} of the rectifier shows good agreement, confirming -10 dB bandwidth, indicating good impedance matching at both the frequency bands as illustrated in Fig. 11(b).

The rectifier's performance was experimentally demonstrated utilizing an RF signal generator to produce controlled RF input signals with power levels ranging from -20 to 16 dBm. The measured results with 4 k Ω recorded, 49.2% efficiency at 0 dBm input, peaking at 54.2% with 5 dBm input power for 2.45 GHz and 26% efficiency at 0 dBm, reaching 28.9% at 3 dBm input power for 5.8 GHz, as shown in Fig. 11(c). Similarly, the output voltage demonstration

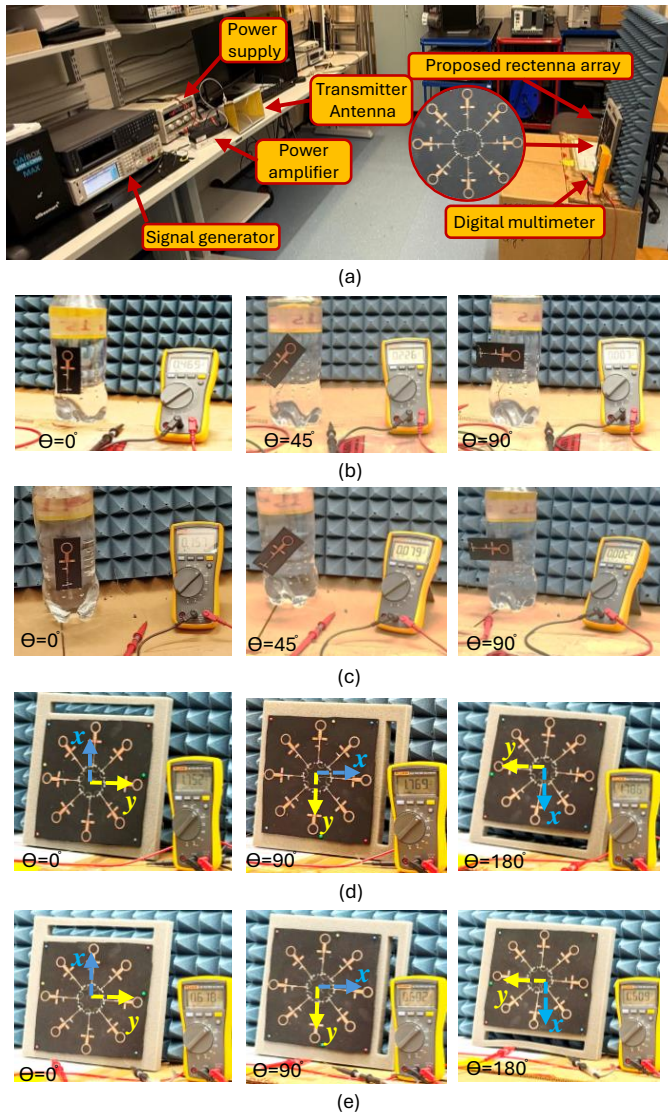


Fig. 12. Demonstration of the single element rectenna and developed rectenna array, (a) experimental setup for the demonstration, (b) single element rectenna demonstration in terms of DC output voltage at 2.45 GHz at various rotation angles, (c) single element rectenna demonstration in terms of DC output voltage at 5.8 GHz at various rotation angles, (d) 8-element Rectenna demonstration in terms of DC output voltage at 2.45 GHz at various rotation angles, (e) 8-element Rectenna demonstration in terms of DC output voltage at 5.8 GHz at various rotation angles.

examined 1.404 V DC output at 2.45 GHz and 1.02 V DC output at 5.8 GHz at 0 dBm input power, as shown in Fig. 11(d). The discrepancies between the simulated and measured results arise mainly from fabrication tolerances, connectors, and soldering losses, and variations in textile properties. Additionally, the lower efficiency observed at 5.8 GHz results from higher diode junction capacitance and stricter impedance matching requirements typical at higher frequencies. Despite these factors, the measured results follow the same trend as the simulations, validating the rectifier performance.

The comprehensive analysis of the proposed dual-band rectifier confirms its potential for seamless integration into RFEH systems. The demonstrated high efficiency values,

reliable performances at two different bands and compatibility with different load resistances, the rectifier emerges a suitable choice for wearable and other low power applications. Additionally, its capability to operate effectively at across low input power levels, highlights the rectifier adaptability, making it suitable solution for harvesting low power ambient RF signals.

IV. DEMONSTRATION OF THE DEVELOPED RECTENNA

This section presents experimental demonstration of the developed rectenna to validate its performance and feasibility. The experiments were performed in two stages, first testing the single-element rectenna, and then evaluating the developed rectenna array. The purpose of the demonstration was to examine the impact of signal polarization and transmission angles on the harvested energy measured by the received DC voltage. The prototypes were examined in a receiving position in different orientations.

A. Single-element Rectenna Demonstration

The initial stage of this testing focuses to evaluate the single-element rectenna by sending and receiving RF signals from various directions. The rectenna was placed on a container filled with MVG's liquid phantom solution (consisted of NaCl, H₂O, DGBE, and Triton X-100), specifically made to mimic the dielectric properties of human tissues, ensuring realistic test conditions. To mimic the operational environment (required input RF at maximum PCE), the experimental setup of this phase is presented in Fig. 12(a). The setup consists of an RF signal generator to produce RF signals at the desired frequencies. The signals were amplified before transmitted to the rectenna at a co-polarization distance of approximately 3 m away, utilizing a high gain horn antenna. The setup conferred the optimal reception of the transmitted signals to the rectenna.

Anritsu portable spectrum analyzer (MS2760A) was used to measure received power levels, where a measurement of -6 dBm at 2.45 GHz and -12 dBm at 5.8 GHz was recorded at the distance, 3 m away from the transmitter antenna.

To evaluate the performance of the system, we started our analysis from a single element rectenna mounted on the cylindrical phantom filled with the tissue mimicking gel, as shown in Fig. 12(b). The rectenna element was initially aligned with the transmitter polarization axis to achieve the polarization matching. In this condition at 2.45 GHz, the highest recorded output DC voltage was 0.461 V. The rectenna was then rotated by 45° to the transmitter polarization axis, with a resulting voltage of 0.228 V recorded (approximately half of the original value). Subsequently, the rectenna was rotated 45° again in a direction to be cross-polarized, resulting in a complete loss of DC output voltage due to complete polarization mismatch, as shown in Fig. 12(b).

Similarly, at 5.8 GHz, when the rectenna element was initially aligned with the polarization axis of the transmitter, the highest recorded output DC voltage was 0.164 V. Upon rotating the rectenna by 45° , the recorded voltage dropped to 0.079 V, approximately half of the initial value. Further rotation by another 45 degrees brought the rectenna into a cross-polarized orientation, resulting in a complete loss of DC

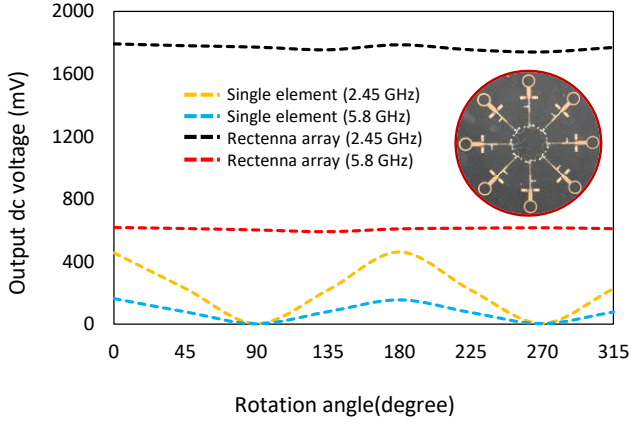


Fig. 13. Demonstration results of the single element and 8-element rectenna, indicating the amplified and stable performance of the developed 8-element over single element at both the selected frequency bands.

output voltage, as shown in Fig. 12(c). This highlights the very strong influence of polarization mismatch on the performance of the single-element rectenna.

B. 8-element Rectenna Demonstration

During the last phase of this study, we examined the overall performance of the 8-element rectenna. The array was positioned at the same distance from the transmitter as was the case with the single element testing, and the received DC voltage was recorded while the array's orientation was varied. The overall RF-to-DC conversion efficiency of the rectenna array can be calculated as

$$\text{PCE} = \left(\frac{P_{\text{DC}}}{P_{\text{RF,in}}} \right) \times 100\%, \quad (7)$$

where P_{DC} is the total DC output power and $P_{\text{RF,in}}$ is the total RF power received by the antenna.

The total received RF power with polarization mismatch can be calculated as

$$P_{\text{RF,in}} = \sum_{n=1}^N P_{\text{incident},n} \cdot \cos^2(\theta_n), \quad (8)$$

where

- N = number of antenna elements,
- $P_{\text{incident},n}$ = incident RF power of element n (before mismatch),
- θ_n = Angle between the polarization of the incident wave and the element,
- and $\cos^2(\theta_n)$ = polarization mismatch efficiency factor.

Similarly, the DC output power can be calculated as

$$P_{\text{DC}} = \frac{V_{\text{DC}}^2}{R_{\text{load}}}, \quad (9)$$

where V_{DC} is the measured output DC voltage and R_{load} is the load resistance.

For the given measurement conditions, the proposed 8-element rectenna having 2 co-polarized, 4 partially misaligned,

TABLE I
MEASURED OUTPUT DC VOLTAGE LEVELS OF SINGLE-ELEMENT (SE) AND RECTENNA ARRAY (RA) AT VARIOUS ROTATION ANGLES

Angle (degree)	2.45 (GHz)		5.8 (GHz)	
	$V_{\text{out_SE}}$ (mV)	$V_{\text{out_RA}}$ (mV)	$V_{\text{out_SE}}$ (mV)	$V_{\text{out_RA}}$ (mV)
0	456	1792	164	618
45	228	1780	79	611
90	4	1771	2	602
135	218	1754	80	591
180	461	1786	156	609
225	218	1754	75	613
270	5	1740	3	616
315	226	1769	78	610

and 2 cross-polarized elements delivered maximum stable output DC voltages of 1.79 V at 2.45 GHz and 0.618 V at 5.8 GHz. These values correspond to overall RF-DC conversion efficiencies of around 77% and 38% at 2.45 and 5.8 GHz, respectively. The array's orientation was varied in 45° increments, and the output DC voltage was examined to be consistent, matching the previous measured values. This pattern was repeated until the array reached its original position, resulting in a consistent measured voltage throughout the angular rotation.

Likewise, the same assessment was carried out maintaining the rectenna in the same position while the transmitter antenna was rotated in 45° increments. Throughout the rotations, a relatively stable DC output voltage of approximately 1.75 V at 2.45 GHz and 0.61 V at 5.8 GHz was examined on every rotation, as shown in Figs. 12(d) and 12(e) respectively. These findings demonstrate stable output performance of the proposed 8-element rectenna, specifically with their consistency in various orientations, unlike the single-element rectenna, where cross- and mismatch polarization significantly produce variations and low output. The circular configuration of the eight monopole elements in the designed configuration enhances polarization diversity. A single-element rectenna can suffer significant power loss in the event of a polarization mismatch, while the proposed array ensures only two elements are cross-polarized at any given time, while the two elements receive the maximum amount of power, remain co-polarized, and the remaining four receive half of the transmission's power. Thus, the array maintains close to 50 % total mutual polarization efficiency regardless of the polarization of the incident wave. Table I presents the output DC voltage levels of the single-element and the 8-element rectenna measured at different rotation angles. Furthermore, the serial DC combination configuration of all the rectifiers results in amplified output voltage compared to a single-element design. We recorded a maximum voltage of 0.46 V under co-polarized conditions with single-element rectenna, while with the 8-element rectenna we obtained an output voltage of 1.75 V, significantly higher and more consistent, approximately 4 times greater. This demonstration validates the effectiveness of the serial DC

TABLE II
COMPARISON WITH THE STATE-OF-THE-ART

Frequency (GHz)	Substrate material	Type of antenna	No. of antenna element	Size (mm ³)	Overall RF-DC efficiency (%)	Angular coverage	Polarization robustness	Publication year
2.45	FR4 (rigid)	Microstrip patch	4	100×240×5	42.4 @ - 10 dBm	No	No	2017 [42]
5.8	FR4 (rigid)	Scoop shaped	8	$\pi \times (67)^2 \times 1.57$	31.2 @ - 12	Yes	No	2022 [43]
5.2	FR4 (rigid)	Endfire and Boresight	8	74×74×1.57	47 – 49 @ - 10 dBm	Yes	No	2022 [29]
0.9 – 5.8	Rogers (rigid)	Endfire Vivaldi	8	Antenna = 460×460×1.5 Rectifier = 120×81.4×1.5	59.5 at 2.4GHz & 20.6 at 5.8GHz @ - 10 dBm	Yes	No	2024 [30]
2.45	Cotton (wearable)	Microstrip patch	5	240×240×1	64.4 @ 10 dBm	Yes	No	2024 [31]
2.45 & 5.8	EPDM (wearable)	Coplanar Monopole	8	$\pi \times (95)^2 \times 3$	77 @ -6 dBm at 2.45GHz and 38 @ -12 dBm at 5.8GHz	Yes	Yes	This work

power combining method for energy harvesting applications. These experimental results validate the reliable performance of the developed rectenna array being able to provide a stable and continuous DC output even when the transmitter is rotated or has become cross-polarized as presented in Fig. 13. The design configuration of the proposed receiving array ensures that the receiver will never be completely cross polarized with a linear transmitter, making it a good candidate for ambient RFEH application.

The performance of the proposed rectenna is compared with the state-of-the-art in Table II. Although previous works have improved angular coverage and supported multiple orientations [42], [43], rigid substrates are difficult to integrate with wearable sensors. Moreover, single-band arrays limit harvesting capability [31], and some multi-band designs have larger footprints unsuitable for compact systems [30]. The proposed 8-element rectenna achieves dual-band operation with wide angular coverage and compact footprints, which delivers higher overall RF-DC PCE under low-power conditions, ensuring better performance in ambient RF environments. Its polarization robustness ensures stable DC output regardless of the transmitter polarization and rectenna orientation, which is essential for reliable sensor operation, while also eliminating the requirement for an intermediate power management circuit.

V. CONCLUSION

This work proposes a textile-based dual-band rectenna array operating at ISM 2.45 and 5.8 GHz for wearable sensor applications. The rectenna was fabricated on a textile substrate using conductive copper-nylon fabric as the conductor. Both simulated and measured results validated consistent performance, achieving peak gains of 2.5 dBi at 2.45 GHz and 5.7

dBi at 5.8 GHz. The measured S_{11} exceeds -15 dB, while S_{12} is well below -20 dB in the two operating frequencies. A dual-band rectifier was also integrated and analyzed, achieving a measured maximum efficiency of 49.2% at 2.45 GHz and 26% at 5.8 GHz, for an input power of 0 dBm. The study also featured the laser-based fabrication process of the proposed rectenna and includes the detailed demonstration of single element and complete array rectenna at various transmitter and receiver rotation angles. These demonstrations validated the array's ability to maintain a stable and amplified DC voltage regardless of orientation variations, highlighting the inherent polarization diversity of the rectenna. The results highlight the significant potential of the proposed rectenna for efficient and battery-free harvesting in challenging indoor environments, providing exciting new developments in the fields of wearable healthcare and smart textiles.

REFERENCES

- [1] A. I. Siam, M. A. El-Affendi, A. A. Elazm, G. M. El-Banby, N. A. El-Bahnasawy, F. E. A. El-Samie, and A. A. A. El-Latif, "Portable and real-time iot-based healthcare monitoring system for daily medical applications," *IEEE Transactions on Computational Social Systems*, vol. 10, no. 4, pp. 1629–1641, 2023.
- [2] M. Riaz and R. Gravina, "Wearable sensor systems to detect biomarkers of personality traits for healthy aging: A review," *IEEE Sensors Journal*, vol. 24, no. 17, pp. 27 061–27 075, 2024.
- [3] M. Qasim Mehmood, M. Adnan, M. Hamza Zulfiqar, K. A. Aljaloud, R. Sarwar, R. Hussain, A. H. Alqahtani, and A. Alomainy, "Textile-based washable multimode capacitive sensors for wearable applications," *IEEE Journal on Flexible Electronics*, vol. 3, no. 10, pp. 445–453, 2024.
- [4] Z. Zhou, W. Tan, J. Cai, Y. Wu, P.-A. Yang, X. Huang, W. Fan, L. Bai, and R. Li, "Wearable 3-d meshed textile pressure sensor for physiological signal monitoring," *IEEE Sensors Journal*, vol. 24, no. 6, pp. 7530–7536, 2024.

- [5] D. Shakhthivel, N. M. Nair, and R. Dahiya, "Nanowires-based stretchable strain sensor for wearable applications," *IEEE Sensors Letters*, vol. 7, no. 6, pp. 1–4, 2023.
- [6] Y. Wang, S. He, Y. Qiu, R. Wu, L. Wang, P. Lu, C. Song, Q. Cheng, and C. Zhang, "Highly efficient broadband ambient energy harvesting system enhanced by meta-lens for wirelessly powering batteryless iot devices," *IEEE Internet of Things Journal*, vol. 11, no. 16, pp. 26916–26928, 2024.
- [7] R. Colucci, I. Mahgoub, H. Yousefzadeh, and H. Al-Najada, "Survey of strategies to optimize battery operation to minimize the electricity cost in a microgrid with renewable energy sources and electric vehicles," *IEEE Access*, vol. 12, pp. 8246–8261, 2024.
- [8] Y. Sun, Y.-Z. Li, and M. Yuan, "Requirements, challenges, and novel ideas for wearables on power supply and energy harvesting," *Nano Energy*, vol. 115, p. 108715, 2023.
- [9] S. Anuradha, R. Manimegalai, and M. Devasena, "Challenges in recycling lead acid battery and lithium-ion battery: A comprehensive review," in *2024 International Conference on Smart Systems for Electrical, Electronics, Communication and Computer Engineering (ICSSECC)*. IEEE, 2024, pp. 101–106.
- [10] F. Z. Peng, C.-C. Liu, Y. Li, A. K. Jain, and D. Vinnikov, "Envisioning the future renewable and resilient energy grids—a power grid revolution enabled by renewables, energy storage, and energy electronics," *IEEE Journal of Emerging and Selected Topics in Industrial Electronics*, vol. 5, no. 1, pp. 8–26, 2023.
- [11] P. Peralta-Braz, M. M. Alamdari, E. Atroshchenko, and M. Hassan, "On the joint optimization of energy harvesting and sensing of piezoelectric energy harvesters: case study of a cable-stayed bridge," *IEEE Transactions on Intelligent Transportation Systems*, vol. 25, no. 1, pp. 559–570, 2023.
- [12] C. Zhang, Z.-G. Liu, S.-H. Liu, and M. Shen, "A self-powered and self-tracking charging multifunctional wireless power transfer system," *IEEE Transactions on Microwave Theory and Techniques*, 2024.
- [13] Z. Wei, X. Shen, G. Qiu, Y. Liu, and J. Liu, "An integrated transfer learning method for power generation prediction of run-off small hydropower in data-scarce areas," *IEEE Transactions on Smart Grid*, vol. 15, no. 1, pp. 1030–1041, 2023.
- [14] A. Khan, S. G. Villar, L. A. D. Lopez, A. Almaleh, A. M. Alqahtani, and R. Alnaimi, "Underwater thermal energy harvesting: Frameworks, challenges, applications and future investigation," *IEEE Access*, 2024.
- [15] M. Mitolo, G. Di Lorenzo, E. Stracqualursi, and R. Araneo, "Electrostatic hazards in power systems," in *2024 IEEE International Conference on Environment and Electrical Engineering and 2024 IEEE Industrial and Commercial Power Systems Europe (EEEIC / ICPS Europe)*, 2024, pp. 1–6.
- [16] K. Niotaki, N. B. Carvalho, A. Georgiadis, X. Gu, S. Hemour, K. Wu, D. Matos, D. Belo, R. Pereira, R. Figueiredo, H. Chaves, B. Mendes, R. Correia, A. Oliveira, V. Palazzi, F. Alimenti, P. Mezzanotte, L. Roselli, F. Benassi, A. Costanzo, D. Masotti, G. Paolini, A. Eid, J. Hester, M. M. Tentzeris, and N. Shinohara, "Rf energy harvesting and wireless power transfer for energy autonomous wireless devices and rfids," *IEEE Journal of Microwaves*, vol. 3, no. 2, pp. 763–782, 2023.
- [17] N. U. Khan, S. Ullah, F. U. Khan, and A. Merla, "Development of 2400–2450 mhz frequency band rf energy harvesting system for low-power device operation," *Sensors*, vol. 24, no. 10, 2024.
- [18] P. Lu, L. Luo, L. Yang, C. Wang, C. Zhang, C. Song, K. Huang, and Y. Huang, "Power-efficient simultaneous wireless information and power transfer (swipt) for batteryless iot devices using a co-designed rectifying metantenna," *IEEE Journal of Microwaves*, vol. 5, no. 1, pp. 34–47, 2025.
- [19] M. C. Chibuike, S. S. Grobbelaar, and A. Botha, "Overcoming challenges for improved patient-centric care: A scoping review of platform ecosystems in healthcare," *IEEE Access*, vol. 12, pp. 14298–14313, 2024.
- [20] P. H. Kyaw, A. B. Lim, C. K. Ho, Y. Y. Koh, and C. L. Kok, "Innovative sustainable solutions for continuous power supply in wearable technology through energy harvesting," in *TENCON 2024 - 2024 IEEE Region 10 Conference (TENCON)*, 2024, pp. 1861–1864.
- [21] N. U. Khan, F. U. Khan, M. Farina, and A. Merla, "Rf energy harvesters for wireless sensors, state of the art, future prospects and challenges: A review," *Physical and Engineering Sciences in Medicine*, vol. 47, no. 2, pp. 385–401, 2024.
- [22] M. Wagih, L. Balocchi, F. Benassi, N. B. Carvalho, J.-C. Chiao, R. Correia, A. Costanzo, Y. Cui, D. Georgiadou, C. Gouveia, J. Grosinger, J. S. Ho, K. Hu, A. Komolafe, S. Lemey, C. Loss, G. Marrocco, P. Mitcheson, V. Palazzi, N. Panunzio, G. Paolini, P. Pinho, J. Preishuber-Pflügl, Y. Qaragoz, H. Rahmani, H. Rogier, J. R. Lopera, L. Roselli, D. Schreurs, M. Tentzeris, X. Tian, R. Torah, R. Torres, P. Van Torre, D. Vital, and S. Beeby, "Microwave-enabled wearables: Underpinning technologies, integration platforms, and next-generation roadmap," *IEEE Journal of Microwaves*, vol. 3, no. 1, pp. 193–226, 2023.
- [23] H. Yahya Alkhalaf, M. Y. Ahmad, H. Ramiah, A. K. M. Zakir Hossain, S. M. Kayser Azam, and A. Thiha, "Flexible meta-patch rectenna array for energizing low-power wearable medical sensors," *IEEE Access*, vol. 12, pp. 121570–121585, 2024.
- [24] W. A. Khan, R. Raad, F. Tubbal, P. I. Theoharis, and S. Iranmanesh, "Rf energy harvesting using multidirectional rectennas: A review," *IEEE Sensors Journal*, vol. 24, no. 12, pp. 18762–18790, 2024.
- [25] W. Tan, Y. He, H. Luo, G. Zhao, and H. Sun, "A wideband high-efficiency side-connected magnetoelectric dipole antenna array using novel feeding technology for w-band," *IEEE Transactions on Antennas and Propagation*, vol. 72, no. 9, pp. 7383–7388, 2024.
- [26] P. Dehghanzadeh, A. Madanayake, H. Zhao, S. B. Venkatakrisnan, and S. Mandal, "A multipoint self-interference canceller for wideband simo/mimo-star full-duplex arrays," *IEEE Transactions on Microwave Theory and Techniques*, vol. 72, no. 4, pp. 2640–2654, 2024.
- [27] U. Olgun, C.-C. Chen, and J. L. Volakis, "Investigation of rectenna array configurations for enhanced rf power harvesting," *IEEE Antennas and Wireless Propagation Letters*, vol. 10, pp. 262–265, 2011.
- [28] S. Shen, Y. Zhang, C.-Y. Chiu, and R. Murch, "Directional multipoint ambient rf energy-harvesting system for the internet of things," *IEEE Internet of Things Journal*, vol. 8, no. 7, pp. 5850–5865, 2021.
- [29] M. Kumar, S. Kumar, and A. Sharma, "A planar orbicular rectenna array system with 3-d uniform coverage for wireless powering of iot nodes," *IEEE Transactions on Microwave Theory and Techniques*, vol. 71, no. 3, pp. 1366–1373, 2022.
- [30] S. Islam, M. Zada, U. R. Iman, and H. Yoo, "Multibeam circular endfire array incorporating highly efficient nona-band rectifiers for iot energy harvesting applications," *IEEE Internet of Things Journal*, vol. 11, no. 12, pp. 22768–22778, 2024.
- [31] M. Zada, U. R. Iman, A. Basir, and H. Yoo, "Battery-free digitally embroidered smart textile energy harvester for wearable healthcare iots," *IEEE Transactions on Industrial Electronics*, vol. 71, no. 8, pp. 9865–9874, 2024.
- [32] N. U. Khan, A. Basir, U. Ali, T. Björninen, and A. Merla, "Enhancing energy harvesting for wearable sensors: A circular 8-element array with spatial diversity," in *2025 19th European Conference on Antennas and Propagation (EuCAP)*, 2025, pp. 1–5.
- [33] C. A. Balanis, *Antenna theory: analysis and design*. John Wiley & sons, 2016.
- [34] [Online]. Available: <https://itis.swiss/virtual-population/tissue-properties/downloads/>
- [35] Skyworks, available: [Online]. Available: https://www.mouser.fi/datasheet/2/472/Surface_Mount_Schottky_Diodes_200041AH-3364421.pdf
- [36] A. Refaei, S. Genevey, Y. Audet, and Y. Savaria, "High-efficiency wide input power range three-phase radio frequency energy harvester for iot applications," *IEEE Transactions on Microwave Theory and Techniques*, vol. 73, no. 3, pp. 1857–1865, 2025.
- [37] D. Le, Y. Kuang, L. Ukkonen, and T. Björninen, "Microstrip transmission line model-fitting approach for characterization of textile materials as dielectrics and conductors for wearable electronics," *International Journal of Numerical Modelling: Electronic Networks, Devices and Fields*, vol. 32, no. 6, p. e2582, 2019.
- [38] Johannes birkenstock gmbh. wuppertal, germany. available: [Online]. Available: <https://www.johannes-birkenstock.de/index.html>
- [39] Staxex produktion- und vertriebs gmbh. bremen, germany. available: [Online]. Available: <https://www.shieldex.de/en/our-products/>
- [40] K. K. Pakkirisami Churchill, G. Chong, H. Ramiah, M. Y. Ahmad, and J. Rajendran, "Low-voltage capacitive-based step-up dc-dc converters for rf energy harvesting system: A review," *IEEE Access*, vol. 8, pp. 186393–186407, 2020.
- [41] M.-K. Law, Y. Jiang, P.-I. Mak, and R. P. Martins, "Miniaturized energy harvesting systems using switched-capacitor dc-dc converters," *IEEE Transactions on Circuits and Systems II: Express Briefs*, vol. 69, no. 6, pp. 2629–2634, 2022.
- [42] D.-J. Lee, S.-J. Lee, I.-J. Hwang, W.-S. Lee, and J.-W. Yu, "Hybrid power combining rectenna array for wide incident angle coverage in rf energy transfer," *IEEE Transactions on Microwave Theory and Techniques*, vol. 65, no. 9, pp. 3409–3418, 2017.
- [43] M. Kumar, S. Kumar, and A. Sharma, "Dual-purpose planar radial-array of rectenna sensors for orientation estimation and rf-energy harvesting at iot nodes," *IEEE Microwave and Wireless Components Letters*, vol. 32, no. 3, pp. 245–248, 2022.



Nasir Ullah Khan (Graduate Student Member, IEEE) received his B.Sc. degree in Telecommunication Engineering from the University of Engineering and Technology, Peshawar, Pakistan, in 2015, and his M.S. degree in Mechatronics Engineering from the same university in 2021. He is currently pursuing a Ph.D. at the Department of Engineering and Geology, G. D'Annunzio University Chieti-Pescara, Italy. His research focuses on RF energy harvesting, printed antennas, wearable and implantable antennas, MIMO antennas, rectifier circuits, and wireless

power transfer for implants.



Toni Björninen (Senior Member, IEEE) received the M.Sc. and Ph.D. degrees in electrical engineering from Tampere University of Technology (TUT), Tampere, Finland, in 2009 and 2012, respectively. He is currently an Associate Professor with the Faculty of Information Technology and Communication Sciences and Vice Director of Tampere Electronics Research Centre, both at Tampere University (TAU), Finland. His research focuses on RF and antenna technology for wireless health, including implantable and wearable antennas, wireless power

transfer, sensors, and RFID-inspired wireless solutions. Dr. Björninen is an author of 200 peer-reviewed scientific articles, and he serves as an Associate Editor in IEEE Antennas and Wireless Propagation Letters.



Abdul Basir (Member, IEEE) was born in Khyber Pakhtunkhwa, Pakistan, in 1989. He earned his B.Sc. degree in Telecommunication Engineering from the University of Engineering and Technology, Peshawar, Pakistan, in 2015. Driven by a passion for research, he pursued and successfully attained a Ph.D. degree in Electronic Engineering from Hanyang University, Seoul, South Korea, in 2021.

Dr. Basir worked as a postdoctoral researcher at Applied Bioelectronics Laboratory Korea from September 2021 to 2024. Currently, he is contributing significantly to the academic and research community as a Postdoctoral Research Fellow at Tampere University, Finland. In this role, he continues to advance knowledge in electronic and biomedical engineering, exploring diverse areas such as implantable antennas and systems, biomedical circuits, wearable antennas, MIMO communication, metamaterials, dielectric resonator antennas, reconfigurable antennas, long-range wireless power transfer, and wireless charging of biomedical implants.

Dr. Basir's commitment to academic excellence extends beyond his research pursuits. He is a prolific reviewer, contributing to the peer-review process for over 200 activities across esteemed journals such as IEEE Transactions on Antenna and Propagation, Advanced Material Technologies, IEEE AWPL, Electronics Letters, Frontier of Information Technology and Electronic Engineering, IEEE Access, IEEE Internet of Things Journal, IEEE Journal of Biomedical and Health Informatics, and more.

In recognition of his outstanding contributions, Dr. Basir has received several prestigious awards, including the Silver Prize for the Best Student Paper Awards in Student Paper Contests from IEEE Seoul Section in 2018 and 2019. Furthermore, a collaborative paper with his participation received the Best Paper Award in 2019 from the IEEE AP/MTT/EMC Joint Chapter Malaysia. His dedication to excellence is further underscored by the Third Prize for the Best Student Paper Competition in 2018 by the Korea Communications Agency (KCA) and the Korean Institute of Electromagnetic Engineering and Science (KIEES).

Dr. Basir's role as a Postdoctoral Research Fellow at Tampere University positions him as a valuable contributor to the global research landscape, emphasizing his commitment to advancing knowledge and shaping the future of bioelectronics and biomedical engineering.



Arcangelo Merla, PhD is a Full Professor of Biomedical Engineering at the University of Chieti-Pescara and Director of the Bioengineering Lab at the same department. He holds a Master's degree in Physics from the University of Bologna and a Ph.D. in Biomedical Technology from the University of Chieti-Pescara. Merla has authored over 260 scientific publications, accumulating more than 7,300 citations. His research focuses on neuroimaging, thermal infrared imaging, and wearable systems for physiological monitoring, contributing significantly

to the fields of neuroscience, affective computing, and human-computer interaction.